Available online at www.sciencedirect.com
SCIENCE DIRECT
Diamond & Related Materials 15 (2006) 904 – 907
DIAMOND AND RELATED MATERIALS
www.elsevier.com/locate/diamond

Plasma 2D modeling and diagnostics of DLC deposition on PET

E. Amanatides, P. Gkotsis, Ch. Syndrevelis, D. Mataras *

Plasma Technology Laboratory, Dept. Chem. Engineering, University of Patras P.O. Box 1407, 26504 Patras, Greece

Available online 19 January 2006

Abstract

The possibility to apply two dimensional (2D) emission spectra of short-lived excited species for estimating the uniformity of production of ions and radicals that have an important role in the deposition of diamond-like coatings on polymeric substrates was investigated. Images of the α-balmer line of atomic hydrogen in CH_4/H_2 discharges were recorded under various total gas pressures and substrate bias voltages to reveal that the increase of the total gas pressure enhances radial non-uniformities of the electron population with energy higher than 16 eV. A comparison between these images and the results of a 2D simulator of CH_4/H_2 discharges shows that the most abundant ions (H_3^+, CH_5^+) and radicals with high reactivity in the gas phase (CH_2, CH, C) present similar axial and radial distribution with these emission maps.

Keywords: Plasma CVD; Bias growth; Reactor modelling; Gas phase reactions

1. Introduction

Recently, the deposition of DLC on polymeric substrates has attracted particular attention for application in plastic optics [1] as well as in food packaging [2] and in biomedical products [3]. Different polymeric substrates as Polycarbonate (PC), Polymethylmethacrylate (PMMA), Polyethylene terephthalate (PET) and Polyvinyl chloride (PVC) substrates have already been coated with amorphous carbon films leading to a significant improvement of their chemical and mechanical surface properties [4–6]. Plasma Enhanced CVD has a definitive advantage for the growth of these films, because it permits the deposition on these sensitive polymer substrates even at room temperature [7]. However, a drawback of this technique is the rather high complexity as a number of physical and chemical processes take place simultaneously, which in turn makes process understanding and its effective control and reproducibility more difficult.

In this sense, there is an emerging need for suitable in situ and non-intrusive plasma diagnostics that can support in an easy and fast way control and optimization of such processes. In this direction, the present work is focused on the implementation of 2D emission spectroscopy as a diagnostic tool for the fast estimation of production and axial/radial distribution of ions and radicals that have an important role in the DLC growth on PET in CH_4/H_2 discharges. The work was performed under well controlled discharge electrical conditions and for different total gas pressures and PET substrate bias voltages and it was complemented by the use of a 2D fluid model of CH_4/H_2 RF discharges.

2. Experimental

The experiments were performed in a cylindrical stainless steel parallel plate chamber with 5.5 mm in diameter electrodes and adjustable electrode separation. The interelectrode space for this series of experiments was kept constant at 25 mm. The chamber is equipped with four quartz windows suitable for optical measurements. The RF electrode is powered by an ENI ACG-3 13.56 MHz RF generator via an L-type matching network, while the substrate electrode is biased using an ENI AT3200 variable frequency generator tuned at 30 KHz. The amount of RF power actually fed into the discharge chamber was determined using an accurate method, employing Fourier transform analysis of power and phase from current and voltage waveform measurements. The excitation voltage and the discharge current signals were measured on the powered electrode lead, using a high impedance 1 : 100 attenuation voltage probe (Hameg, model AZ92) and a 0.1 Ω transfer impedance RF current probe (FCC model F-35-1). The measured voltage and current waveforms were then transformed to the ones at the surface of the powered electrode using an equivalent circuit comprising only experimentally

* Corresponding author. Tel.: +30 2610 997857.
E-mail address: dim@plasmatech.gr (D. Mataras).

0925-9635/$ - see front matter © 2005 Elsevier B.V. All rights reserved.
doi:10.1016/j.diamond.2005.11.031

determined components [8]. The substrate bias voltage was measured using another high impedance 1:10 attenuation voltage probe (Hameg, model AZ92).

The setup used to record the emission spectra and 2D emission images consists of a cylindrical or a focusing achromatic lens, an imaging spectrograph and an iCCD detector (Andor, iStar734). The dimensions of the quartz window were higher than the discharge area allowing the recording of the emission from the whole discharge area either in the axial or the radial direction. Emission spectra of CH_4/H_2 discharges were obtained for the wavelengths between 200 nm and 700 nm. Emission 2D images were recorded for the CH radical ($A^2\Delta \rightarrow X^2\Pi$, 431 nm), H_2 ($d^3\Pi_u \rightarrow a^3\Sigma_g^+$, 612 nm), H_α ($n=3 \rightarrow n=2$, 656 nm) and H_β ($n=4 \rightarrow n=2$, 486 nm) by using suitable interference filters.

3. Model

The 2D self-consistent model has been described in detail in Refs. [9,10]. Briefly, the model uses the particle, momentum and energy balances obtained from moments of the Boltzmann transport equation, coupled with Poisson's equation for a self-consistent calculation of the electric field.

Special attention was given in the detailed gas phase chemistry and the DLC growth by including in the model 27 species (radicals, ions, neutrals, excited species), 5 surface species (physisorpted sites and bulk material), 58 gas phase reactions (electron – molecule, radical – molecule, radical – radical, ion – neutral) and 44 surface reactions (physisorption, chemisorption, desorption, sputtering and stitching). The required collision cross-sections were taken from Refs. [11,12] and the set of reaction rate constants from Ref. [13]. For the plasma – surface interaction it was assumed that all radicals reaching the surface are initially physisorpted with probabilities taken from Ref. [14]. Then a number of reactions were considered which can lead to spontaneous desorption, chemisorption, sputtering and ion enhanced chemisorption. The rate constants of these reactions, the sputtering yields and the ion sticking probability were taken from Refs. [14,15]. For the spatial discrimination of the transport equations a Sharfetter – Gummel scheme was applied and in order to avoid instabilities the distance between the two electrodes was divided to 40 grid points whereas the radial direction was divided to 50 grid points.

4. Results and discussion

Experimental measurements of the power dissipation in the discharge and 2D optical emission spectra together with the fluid model were applied at different CH_4/H_2 total gas pressures (0.25 to 1 Torr) and for different substrate bias voltages (0 to 350 V peak to peak). The fraction of CH_4 in the gas mixtures was set at 8% in all cases, the total gas flow rate at 50 sccm and the distance of the RF electrode from the PET surface at 2.5 cm. In these conditions, previous work of this group [16] has shown that the decrease of pressure or/and the increase of the substrate bias for the same applied voltage (400 V peak to peak) results in an enhancement of the power dissipation in the discharge. This trend was also reproduced by the simulation and an excellent agreement was found between the model calculations and the experiment concerning the electrical properties of the discharge. For instance, in the case of 0.25 Torr and unbiased conditions the calculated power was 4.1 W and the measured 3.8 W. For the same pressure but for 350 peak to peak substrate bias the calculated power was 7.2 W and the measured 6.9 W. This agreement, which is very important for a reliable application of the model, was achieved only after the introduction of almost all the electron collision reactions that can take place with CH_4 and H_2 but also with higher homologues as C_2H_2, C_2H_4, C_2H_6 and C_3H_6 that are produced in the discharge. The use of simplified gas phase chemistry schemes always led to model underestimation of the total power dissipated in the discharge.

In the same work [15], time-averaged 1D spatially resolved optical emission spectroscopy of CH excited species ($A^2\Delta - X^2\Pi$) and α-balmer line of atomic hydrogen were found to be rather sensitive in the variations of either the total gas pressure or the substrate bias voltage. However, no information was obtained on the radial distribution of the species, which will affect the uniformity of the deposited layers. Thus, Fig. 1(a), (b) and (c) presents the time-averaged 2D images of the H_α line

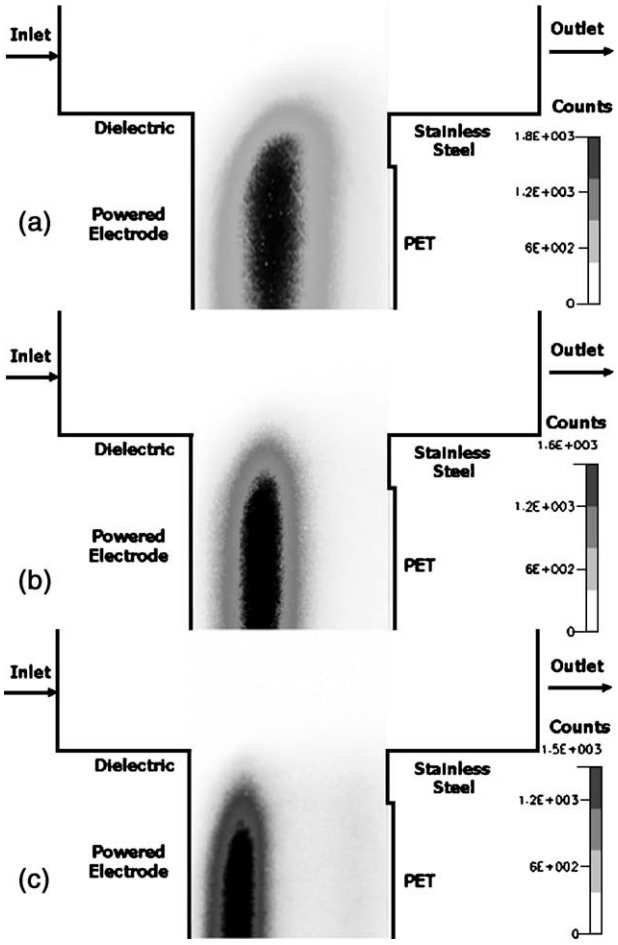

Fig. 1. 2D emission images of α-balmer line of atomic hydrogen in 8% CH_4 in H_2 discharges, 400 V peak to peak RF voltage, and 350 V substrate bias voltage and for total gas pressures of (a) 0.25 Torr (b) 0.5 Torr and (c) 1 Torr.

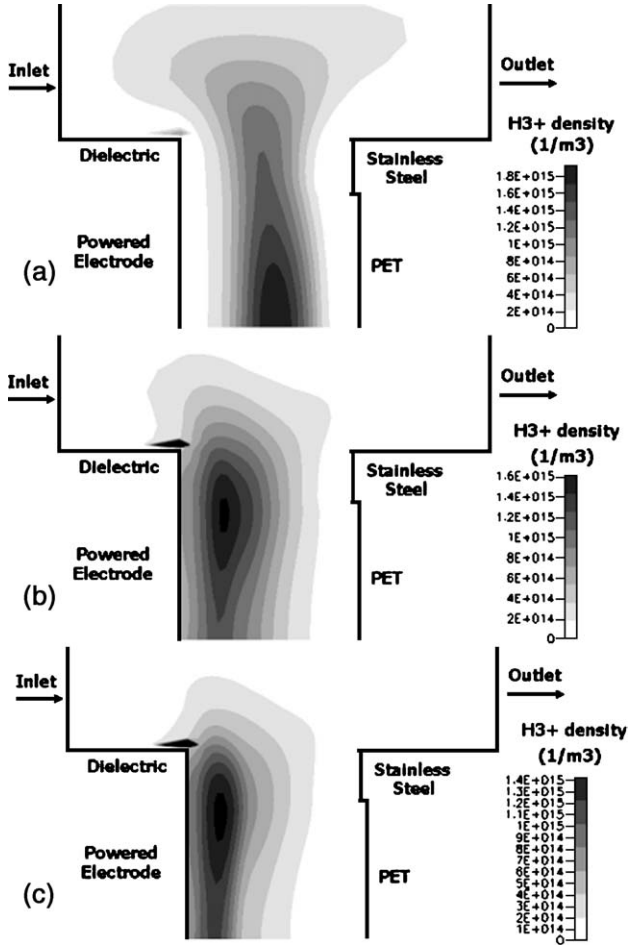

Fig. 2. Model predicted 2D maps of H_3^+ density in conditions of Fig. 1 and for total gas pressures of (a) 0.25 Torr (b) 0.5 Torr and (c) 1 Torr.

at the total gas pressures of 0.25, 0.5 and 1 Torr, respectively. This line was preferred as it has a rather short life-time (15 ns) [17] and the recorded emission signal can be assumed to reflect the net de-excitation and consequently the net excitation rate by the electron population having energy above 16.6 eV (process threshold). This was also confirmed by the model results, where the quenching rate of $Ç_\alpha$ with either H_2 or CH_4 [17] was found to be about at least one order of magnitude less compared to the spontaneous de-excitation rate over the entire range of pressures. In addition, the production of H_α through dissociative excitation of CH_4 can be neglected due to the low CH_4 concentration and the much higher energy threshold of the process (21.3 eV). Thus, the images of Fig. 1 are representative of the net electron population with energy higher than 16.6 eV and as one can observe the increase of pressure leads to a localization of this population near the RF electrode and also to a less uniform distribution in the radial direction. In general, the increase of pressure as found to shrink the discharge area and to keep electrons having enough energy to dissociate CH_4 or H_2 far from the PET surface. For the axial direction, the optimum was found at 1, 0.8 and 0.5 cm for the pressures of 0.25, 0.5 and 1 Torr, respectively. For the radial direction, non-uniformities start to appear at distances higher than 2.5 cm from the axis of the RF electrode at the pressure of 0.25 Torr, for distances higher than 2.2 cm for the pressure of 0.5 Torr and for distances higher than 1.25 cm at 1 Torr. Taking into account that the radius of the PET substrate is 2.25 cm, these non-uniformities in the radial direction are expected to affect the deposition process only at pressures higher than 0.5 Torr.

Moreover, in order to have a better estimation of the correlation between the results of the 2D emission images with the distribution of species that have a significant role in the deposition of DLC, the model results concerning the species' distribution were analyzed and compared with the emission results. In the growth of DLC, both ions (CH_5^+,CH_4^+, CH_3^+, H_2^+, H_3^+) through sputtering or direct incorporation and radicals (C, CH, CH_2, CH_3, C_2H_5) through physisorption and chemisorption may have an important contribution. For the ions, in the present case of highly diluted CH_4 in H_2, the model predicts that H_3^+ is the dominant ion in the discharge as it is produced from the very fast reaction of H_2^+ with H_2 and contributes to slower reactions with CH_4, C_2H_6 and C_2H_4. Thus, Fig. 2(a), (b) and (c) shows the time-averaged 2D maps of the H_3^+ density for the conditions of Fig. 1. The increase of pressure results in a slight drop of the H_3^+ density mainly due to an enhancement of the reaction rate of this ion with methane. As in the case of the emission images, the increase of pressure leads to a shift of the H_3^+ density towards the RF electrode and to a shrinking of the

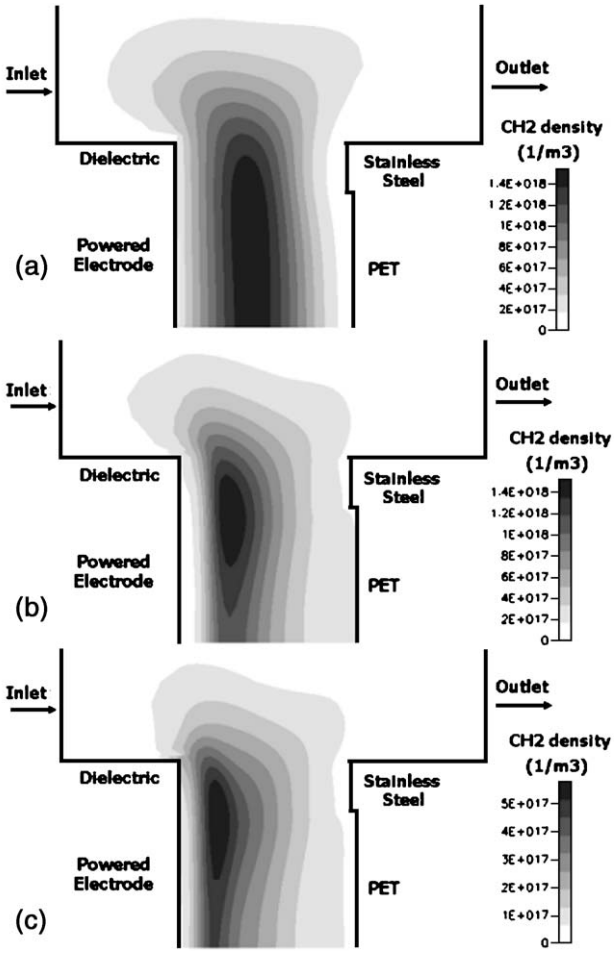

Fig. 3. Model predicted 2D maps of CH_2 density in conditions of Figs. 1 and 2 and for total gas pressures of (a) 0.25 Torr (b) 0.5 Torr and (c) 1 Torr.

maps in the radial direction. It is worth noting that in the axial direction the optimum of H_3^+ density is located at 1.2, 0.7 and 0.5 cm at the pressures of 0.25, 0.5 and 1 Torr, respectively, i.e. very close to the optimum values obtained by the emission images (Fig. 1). Concerning the radial direction, the model predicts higher non-uniformities compared to the emission results but reproduces very well the significant enhancement of this phenomenon with the increase of pressure.

Namely, at 0.25 and for the axial position where density is optimized, differences of about 20% in the radial direction were calculated for the H_3^+ density. For 0.5 Torr these differences exceed 35% while at 1 Torr they become higher than 40%. Taking into account the fact that CH_5^+ ions (the dominant hydrocarbon ion in the discharge) follow the same distribution as H_3^+, it can be stated that emission 2D maps reflect fairly well the distribution of all the ions in the discharge.

The same procedure that was followed in the case of ions was also performed for the free radicals included in the model (C, CH, CH_2, CH_3 and C_2H_5). These radicals have different gas phase reactivity and more precisely C, CH, CH_2 undergo reactions with rates of $\sim 10^{-10}$ cm^3/s with stable molecules (CH_4, C_2H_4, C_2H_2). On the other hand, CH_3 and C_2H_5 react between them or between themselves with rates of $\sim 10^{-12}$ cm^3/s.

Fig. 3(a), (b) and (c) presents the 2D maps of CH_2 density for the conditions of Figs. 1 and 2 and as one can observe the distribution of this highly reactive in the gas phase radical is pretty much the same with either the emission images or the maps of the H_3^+ ion density. For this radical, the axial density optimum position coincides with the emission images at each pressure. As for the radial non-uniformities, the model predicts almost no variations in CH_2 density at 0.25 Torr but an enhancement of the density gradients at 0.5 and 1 Torr (~25%). Similar maps were also calculated for the CH and C radicals, allowing thus to state that emission images can be used for the prediction of the distribution and the non-uniformities of the highly reactive radicals' density. On the other hand, for the CH_3 and C_2H_5 a good comparison between model and emission maps was found only in the lower pressure of 0.25 Torr. At higher pressures and due to the fact that the distribution of these radicals is governed by diffusion, strong deviations were found between the images and model calculations. Based on this discussion we can summarize that 2D emission spectroscopy can be a powerful tool for optimizing the DLC deposition process in terms of radicals and ions uniform production. Further work is in progress in order to correlate the results of the experimental measurements and of the model concerning the radial and axial distribution of species with film properties as thickness uniformity, roughness and sp^2 to sp^3 bonds' ratio variation.

5. Conclusions

Two dimensional emission images of H_2 ($d^3\Pi_u \rightarrow a^3\Sigma_g^+$, 612 nm), H_α ($n=3 \rightarrow n=2$, 656 nm) and H_β ($n=4 \rightarrow n=2$, 486 nm) were recorded in CH_4/H_2 discharges under various gas pressures and PET substrate bias voltages. Analysis of the results of H_α images, chosen on the basis of the life-time of the state and the quenching rate from either CH_4 or H_2, revealed that under these conditions the emission 2D maps of this line reflect the population of electrons having energy above 16 eV. This population was found to be displaced towards the RF electrode and to be less uniformly spread in the radial direction of the discharge with the increase of pressure.

The results of the 2D emission of H_α were then correlated to the calculations of the 2D fluid model of CH_4/H_2 discharges concerning the species density distribution in both the axial and the radial direction. A very good agreement was found for all pressures between the emission measurements and the model calculations concerning the density optimum of the most abundant ions (H_3^+, CH_5^+) in the axial direction and the non-uniformities in the radial direction. Concerning the radicals, the maps of H_α emission and maps of radicals with high reactivity in the gas phase (CH_2, CH, C) were almost identical, while the distribution of species with low gas phase reactivity (C_2H_5, CH_3) show good agreement with emission images below 0.5 Torr.

These results indicate that 2D emission of short-lived species can be a powerful tool for a fast optimization of the DLC deposition process in terms of species uniformity and production.

References

[1] A. Kimura, H. Kodama, T. Suzuki, J. Vac. Sci. Technol., A 21 (2003) 515.
[2] Y.B. Guo, F.C.N. Hong, Diamond Relat. Mater. 12 (2003) 946.
[3] Y. Ohgoe, K.K. Hirakuri, K. Tsuchimoto, G. Friedbacher, O. Miyashita, Surf. Coat. Technol. 184 (2004) 263.
[4] X.T. Zhou, S.T. Lee, I. Bello, A.C. Cheung, D.S. Chiu, Y.W. Lam, C.S. Lee, K.M. Leung, X.M. He, Surf. Coat. Technol. 123 (2000) 273.
[5] N.K. Cuong, M. Tahara, N. Yamauchi, T. Sone, Surf. Coat. Technol. 174–175 (2003) 1024.
[6] T. Tanaka, M. Yoshida, M. Shinohara, T. Takagi, J. Vac. Sci. Technol., A 20 (2002) 625.
[7] J. Robertson, Mater. Sci. Eng., R Rep. 37 (2002) 129.
[8] N. Spiliopoulos, D. Mataras, D. Rapakoulias, J. Vac. Sci. Technol., A 14 (1996) 2757.
[9] B. Lyka, E. Amanatides, D. Mataras, appeared in Proc. of 19th European Photovoltaic Solar Cell Energy Conf. and Exhibition Paris — France 2004.
[10] E. Amanatides, B. Lykas, D. Mataras, IEEE Trans. Plasma Sci. 33 (2005) 372.
[11] ftp://jila.colorado.edu/collision_data/.
[12] D.K. Davies, L.E. Kline, W.E. Bies, J. Appl. Phys. 30 (1989) 3311.
[13] I.B. Denysenko, S. Xu, J.D. Long, P.P. Rutkevych, N.A. Azarenkov, K. Ostrikov, J. Appl. Phys. 95 (2004) 2713.
[14] N.V. Mantzaris, E. Gogolides, A.G. Boudouvis, A. Rhallabi, G. Turban, J. Appl. Phys. 79 (1996) 3718.
[15] C. Cavalloti, M. Masi, S. Carra, J. Electrochem. Soc. 145 (1998) 4332.
[16] E. Amanatides, D. Mataras, Diamond Relat. Mater. 14 (2005) 292.
[17] F. Tochikubo, T. Makabe, S. Kakuta, A. Suzuki, J. Appl. Phys. 71 (1992) 2143.